Palaeogeography, Palaeoclimatology, Palaeoecology 417 (2015) 371–378

Contents lists available at ScienceDirect

Palaeogeography, Palaeoclimatology, Palaeoecology

journal homepage: www.elsevier.com/locate/palaeo

Terrestrial evidence for a two-stage mid-Paleocene biotic event

Ethan G. Hyland [a,*], Nathan D. Sheldon [a], Jennifer M. Cotton [b]

[a] Department of Earth and Environmental Sciences, University of Michigan, 1100 N. University Ave., Ann Arbor, MI 48109, USA
[b] Department of Geology and Geophysics, University of Utah, 115 South 1460 East, Salt Lake City, UT 84112, USA

ARTICLE INFO

Article history:
Received 1 July 2014
Received in revised form 24 September 2014
Accepted 29 September 2014
Available online 5 October 2014

Keywords:
Paleosols
Paleoclimate
Paleocene
Mid-Paleocene biotic event
Carbon

ABSTRACT

Marine records of the Paleocene indicate a series of hyperthermal events characterized by significant climatic and carbon cycle variability, but there are few comparable continental records. The mid-Paleocene biotic event (MPBE) is a recently described interval defined by a rapid negative carbon isotope excursion and major short-term changes in marine ecosystems, but it is as yet unclear whether the event was globally important. Here we present the first terrestrial paleoenvironmental record of the MPBE based on paleosols that document rapid and short-lived increases in temperature and precipitation and resultant shifts in plant assemblages concomitant with substantial carbon isotope excursions. The new record indicates that carbon cycle changes during the early late Paleocene may have resulted in a two-stage transient hyperthermal event that caused a significant perturbation to both the regional climate and terrestrial ecology of South America in addition to the major biotic event (MPBE) previously recognized in marine records. Overall, this suggests that the MPBE may have been a global climate event with far-reaching environmental impacts in both the marine and terrestrial realms.

1. Introduction

The series of Paleogene hyperthermals that have been described represent the most abrupt and extreme instances of climatic warming during the Cenozoic, and are likely the best geologic analogues for anthropogenic climate change (McInerney and Wing, 2011; NRC, 2011). Identifying climatic and ecological responses to these events on land allows for effective predictions of future global climate patterns and their impacts on terrestrial biomes and ecosystem services (NRC, 2011; IPCC, 2014). Terrestrial paleoclimate records of these events are currently limited to major events and come primarily from the northern hemisphere (Wing et al., 2005; McInerney and Wing, 2011), leaving the interpretation of most Paleogene events to marine proxy records (e.g., Hollis et al., 2005; Zachos et al., 2010).

One such event is the mid-Paleocene biotic event (MPBE) or early late Paleocene event, which is a rapid climate change event accompanied by a major biological turnover during the mid-Paleocene, immediately preceding the Selandian–Thanetian stage boundary (Bralower et al., 2002; Petrizzo, 2005; Westerhold et al., 2011). The MPBE is identified in marine cores (Shatsky Rise, Leg 198; Walvis Ridge, Leg 208) by a distinct drop in carbonate preservation and a substantial change in microfossil assemblages (Bralower et al., 2002; Zachos et al., 2004). The event has also been described from marine outcrop sections such as the Zumaia locality (Spain), which records a sizeable negative carbon isotope excursion (CIE) in addition to changes in carbonate preservation and in microfossil assemblages (Bernaola et al., 2007). As a result of these records, researchers have suggested that a large mass of isotopically depleted carbon (methane hydrate) may have been released into the ocean–atmosphere system, triggering carbonate dissolution and global hyperthermal conditions that may have contributed to a substantial restructuring of both planktic and benthic marine environments (e.g., Thomas and Zachos, 2000; Petrizzo, 2005; Bernaola et al., 2007; Westerhold et al., 2011).

Despite potentially significant evolutionary implications of the MPBE and associated hyperthermal conditions (e.g., Thomas and Zachos, 2000; Petrizzo, 2005), the event remains undocumented on land and poorly described in the southern hemisphere. In order to address these issues, we present a multiproxy terrestrial record of the age and climatic/ecological conditions at Cerro Bayo (northwest Argentina) during a two-stage hyperthermal event within the early late Paleocene using magnetostratigraphy, whole rock and stable isotope geochemistry, and phytolith-based paleovegetation reconstruction, and link these transient terrestrial climatic and ecological conditions to well-described records of the marine MPBE interval.

2. Setting and methods

2.1. Geologic setting

Cerro Bayo is located along the western margin of the Salta Basin (Fig. 1), a failed rift basin in northwestern Argentina that formed during the Cretaceous and early Paleogene, and which was later filled by

* Corresponding author at: Department of Earth and Space Sciences, University of Washington, Johnson Hall Rm 070- Box 351310, 4000 15th Ave NE, Seattle, WA 98195, USA. Tel.: +1 207 543 1167.
E-mail address: hylande@uw.edu (E.G. Hyland).

http://dx.doi.org/10.1016/j.palaeo.2014.09.031
0031-0182/

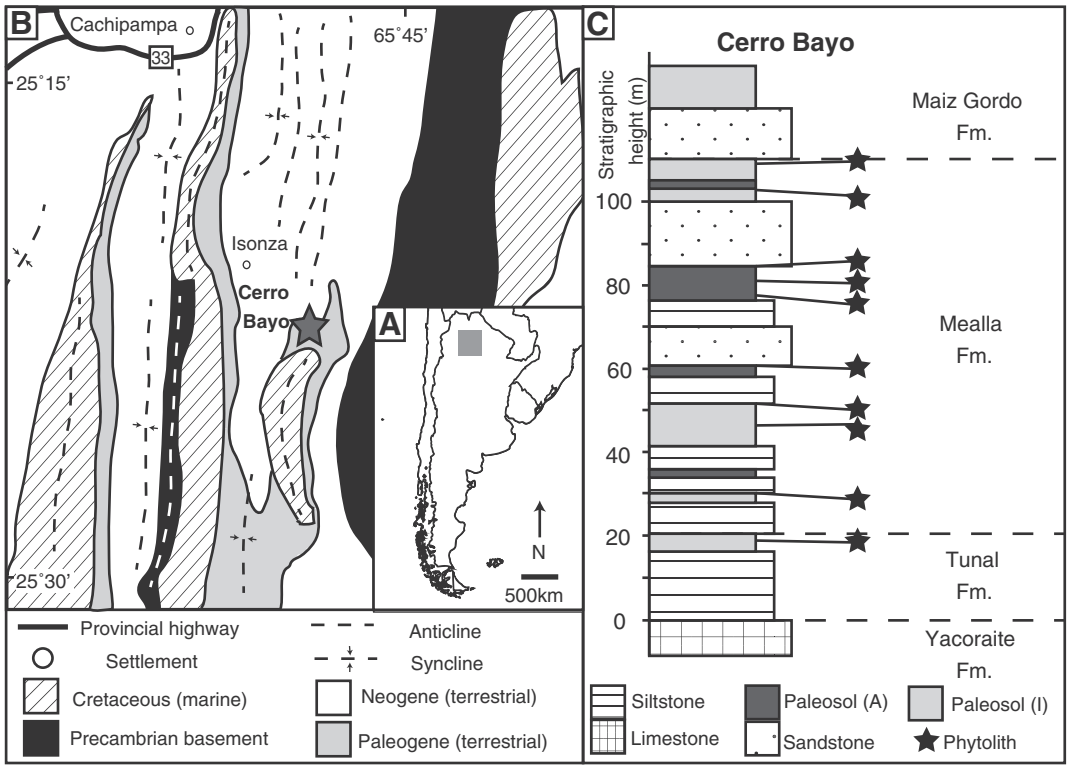

Fig. 1. Map of locality within Argentina (A), with local geology of the Salta Basin (B; modified from Salfity and Monaldi, 2006), and stratigraphy of the lower Cerro Bayo section (C). Stratigraphy indicates sampled paleosols and their identified pedotypes (A = Alfisol, I = Inceptisol), as well as the sampling levels for phytolith assemblages.

material from the topographically higher Puna and Pampean Arch regions during the Araucana-Mirano Orogeny (Marquillas et al., 2005; Salfity and Monaldi, 2006). While the basin now resides between approximately 24 and 25°S, during its formation it was positioned at temperate latitudes around 40°S (±5°; Scotese, 2000), similar to many Paleogene terrestrial records from the northern hemisphere (e.g., McInerney and Wing, 2011). The Cerro Bayo section is composed of the Balbuena and Santa Bárbara Subgroups, and includes the Tunal and Mealla Formations, which are primarily mudrocks and sandstones that were deposited along the margin of paleolake Maíz Gordo/Alemanía (Fig. 1). Many of these are floodplain deposits that show substantial evidence of pedogenesis (Marquillas et al., 2005; Do Campo et al., 2007), with at least 15 distinct and well-defined paleosol profiles exhibiting a range of pedogenic development (Fig. 1; Data Repository Figure DR1). The paleosols in these formations preserve discernable horizonation throughout, and many contain argillic, gleyed, and carbonate horizons (Data Repository Figures DR1 and DR2). Based on this horizonation and on pedogenic features such as root traces and burrows (Data Repository Figure DR2), these paleosols are classified as Inceptisols and Alfisols using the USDA Soil Classification scheme (Soil Survey Staff, 1999).

2.2. Age model

Magnetostratigraphic sampling of the lower ~110-meters of the Cerro Bayo section was performed to determine normal and reversed polarity intervals, and to tie the local polarity pattern to the geomagnetic polarity timescale (GPTS; Gradstein et al., 2012). Block samples of multiple lithologies (siltstone, fine sandstone, limestone) were collected in the field and oriented by hand using a Brunton Field Transit compass on cleared bedding planes. Paleomagnetic specimen cores were drilled from oriented hand samples using a drill press, and further analyses were conducted at the University of Michigan Paleomagnetism Laboratory. Stepwise thermal demagnetization from 100 to 700 °C (Fig. 2; regular 50 °C steps to 500 °C, and regular 25 °C steps thereafter) used an ASC thermal demagnetizer and a 2G cryogenic magnetometer. Analysis of 66 sampling levels (~1.8 m interval) yielded reliable characteristic remanent magnetization (ChRM) directions at 60 levels (Data Repository Table DR1). ChRM directions from vector endpoint diagrams were calculated on a minimum of 5 measurements (250–600 °C) using Virtual Paleomagnetic Directions (VPD) software (Ramón and Pueyo, 2008). Sample means were calculated for ~3 individual cores per sample level, and samples with a mean angular deviation (MAD) >15° were rejected from further analysis; all other samples were bedding and tilt corrected, and statistical models were applied to verify data quality (e.g., reversals test, Fisher means; Ramón and Pueyo, 2008).

2.3. Geochemical methods

Bulk samples for the stable isotopic analyses of paleosol organic material ($\delta^{13}C_{org}$) were collected from trenches (dug to at least 20 cm depth) to avoid modern contamination and were treated with dilute HCl (~7%) to remove all reactive detrital or pedogenic carbonate (e.g., Koch, 1998; Cotton et al., 2012), and then rinsed in distilled water before being dried and packed in tin capsules. Samples were then analyzed on a Costech elemental analyzer attached to a Thermo Delta V + isotope ratio mass spectrometer at the University of Michigan's Stable Isotope Laboratory where results are reported in per mil relative to VPDB (IAEA standards) with an analytical uncertainty <0.1‰, and where replicate analyses (at least two per sample) had standard deviations <0.25‰ (Data Repository Table DR2).

Elemental compositions of whole rock samples from the B-horizons of paleosols (n = 14) were measured via X-ray fluorescence analysis at ALS Chemex Lab (Vancouver, BC), where analytical uncertainty is maintained at ~0.001% and duplicate analyses of bulk samples had standard deviations <0.1%. Major elemental composition ratios (CIA-K, salinization) were used as inputs for mean annual precipitation and mean annual temperature climofunctions derived from modern soil weathering profile relationships (Sheldon et al., 2002). These climofunction relationships have been robustly applied throughout

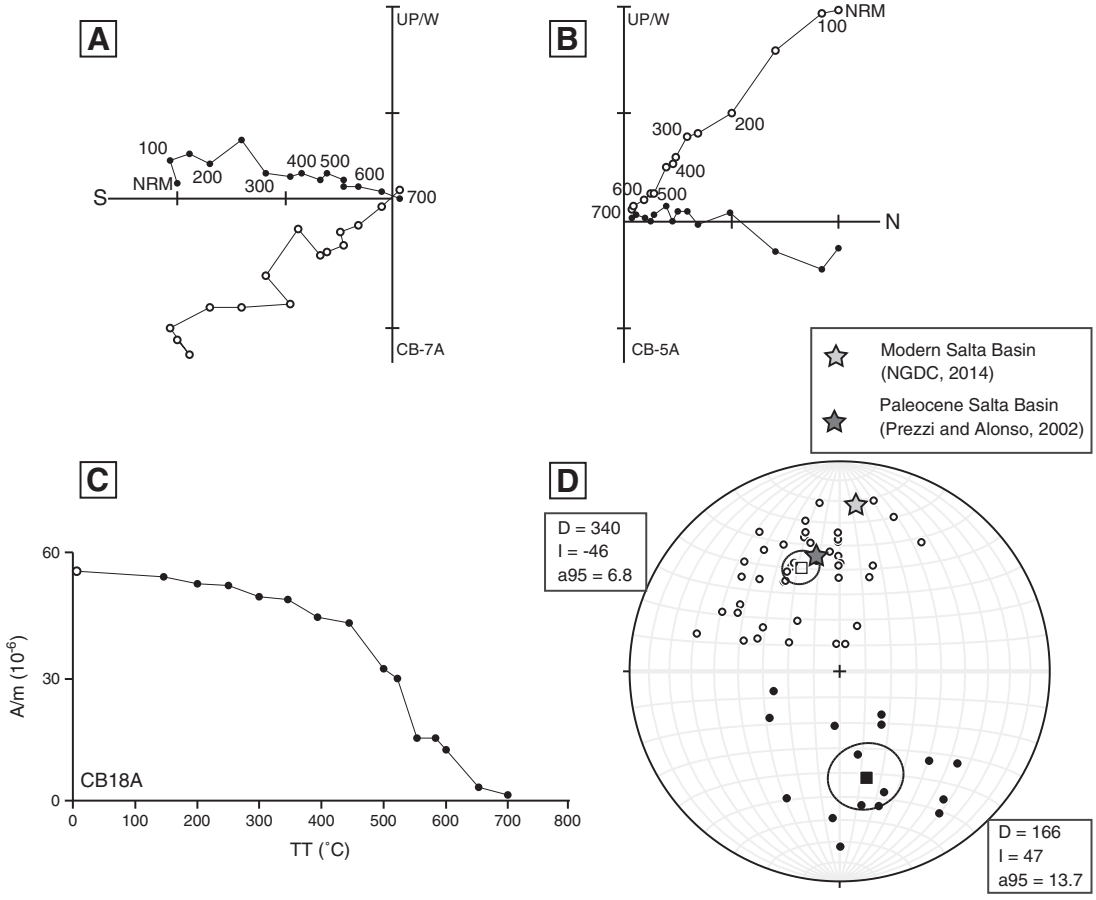

Fig. 2. Magnetostratigraphic results including: example vector endpoint diagrams for normal (A) and reversed (B) samples with thermal demagnetization steps; example thermal decay diagram for a fully demagnetized sample (C); and (D) a stereoplot of characteristic remanent magnetizations (ChRM) for all samples with Fisher mean values (squares), a95 circles, and modern and Paleocene poles for NW Argentina.

the Cenozoic (e.g., Retallack, 2007; Torres and Gaines, 2013) on many continents (e.g., Thomas et al., 2011; Sheldon et al., 2012), and despite substantial standard error on absolute mean annual temperature and precipitation estimates (MAT = ±4 °C; MAP = ±182 mm yr^{-1}), both relationships have been demonstrated to describe smaller-magnitude changes reliably when used as a vector-of-change or trending measurement (e.g., Sheldon and Tabor, 2009; Hyland and Sheldon, 2013). In order to verify trends described by these methods, these results were also compared to the magnitude of change in: 1) mean annual temperature estimates derived from Inceptisol clayeyness (e.g., Sheldon, 2006), and 2) mean annual precipitation estimates derived from depth-to-Bk horizon measurements (e.g., Retallack, 2005), wherever possible within the Cerro Bayo section. Given the limitations of the absolute estimates and of comparing error between methods (physical parameter versus chemical composition), results are expressed as the magnitude of change for climatic conditions through this time period using average estimates of mean annual temperature and precipitation from the underlying Tunal Formation as a pre-event baseline for the Paleocene (see Data Repository Table DR3).

2.4. Phytolith analysis

Selected paleosol A horizons (n = 10) were processed for phytoliths via standard disaggregation-flotation methods (e.g., Strömberg et al., 2007). Isolates were mounted on slides and counted/photographed using a Leica petrographic microscope (400–1000× magnification). Phytolith morphologies were identified under rotation on immersion-oil slides based on both modern reference collections (Selena Smith, University of Michigan; e.g., Chen and Smith, 2013) and paleo-collections (Strömberg, 2003, 2005; Strömberg et al., 2007). Phytolith morphotypes were then categorized by plant functional group based on the affinities defined in modern reference collections (see Data Repository Table DR4), and assemblage composition was calculated by group as a percentage of the total diagnostic count (>200 per sample; e.g., Strömberg et al., 2007). Due to the consistent pedotype of the sampled paleosols (Inceptisols) and the broad functional group comparisons employed, taphonomic biases are assumed to be minimal, and standard error for vegetation composition is estimated at ±2% (Hyland et al., 2013).

3. Results

3.1. Age model

Samples were universally demagnetized between 500 and 700 °C, suggesting a primary ChRM carrier of magnetite and/or hematite (Fig. 2C), and resultant vectors define normal and reversed polarity stable components with a final average MAD of 7.4° (Fig. 2A and B). These components cluster into two nearly antipodal groups (Fig. 2D) with Fisher means at D = 340°, I = −46° (a95 = 6.8) and at D = 166°, I = 47° (a95 = 13.7). The two poles pass a basic reversals test (Fig. 2D), and pole mean directions are distinct from the modern direction for Cerro Bayo (NGDC, 2014) and also fit the expected Paleocene direction based on paleogeographic reconstructions (Fig. 2D; e.g., Scotese, 2000; Prezzi and Alonso, 2002). When plotted stratigraphically, samples define polarity zones for constructing a local polarity timescale (LPTS), each of which were defined by multiple stable sample levels (>3) and a lack of ambiguous polarity zones (i.e., single-level reversals, core

mismatches), which suggests a primary origin for all of the established intervals (Fig. 3).

These magnetozones show a reliable polarity pattern of a reversed and a normal interval during the Tunal Formation (Fig. 3), followed by a substantial disconformity or hiatus as inferred from sedimentological changes/features (e.g., Marquillas et al., 2005), and then a pattern of reversed, normal, and reversed intervals during the Mealla Formation (Fig. 3), again followed by a substantial disconformity or hiatus as inferred from sedimentological changes/features (e.g., Marquillas et al., 2005). Based on palynological evidence from lacustrine muds throughout the Tunal Formation, the formation correlates to the late Danian stage of the early Paleocene (e.g., Quattrocchio et al., 1997; Quattrocchio and Volkheimer, 2000). Combined with magnetostratigraphic data (Figs. 2 and 3), this suggests that the Tunal Formation primarily falls within chron C27n, and as a result, likely spans roughly 62.7–62.4 Mya based on linear interpolation of sedimentation rates between polarity boundaries and reasonable lacustrine deposition rates for the basin during this period (e.g., Turner et al., 1979; Gradstein et al., 2012).

Based on palynological evidence from lacustrine muds at the base of the Mealla Formation, this formation correlates to the Selandian stage of the middle Paleocene (e.g., Quattrocchio et al., 1997; Quattrocchio and Volkheimer, 2000). Further evidence from mammalian fossils within the Mealla Formation (e.g., *Simpsonotus*; Pascual, 1981) suggests that the formation is pre-Itaboraian within the South American Land Mammal Ages (e.g., Clyde et al., 2014; Woodburne et al., 2014), which also provides a middle Paleocene age. Combined with magnetostratigraphic data (Figs. 2 and 3), this suggests that the Mealla Formation contains the end of chron C26r, as well as the entirety of chron C26n, and the beginning of chron C25r, and as a result, likely spans roughly 59.4 to 58.9 Mya based on the linear interpolation of sedimentation rates between polarity boundaries and the associated higher deposition rates of fluvial and overbank sedimentation during this period (Fig. 3; e.g., Marquillas et al., 2005; Salfity and Monaldi, 2006; Gradstein et al., 2012).

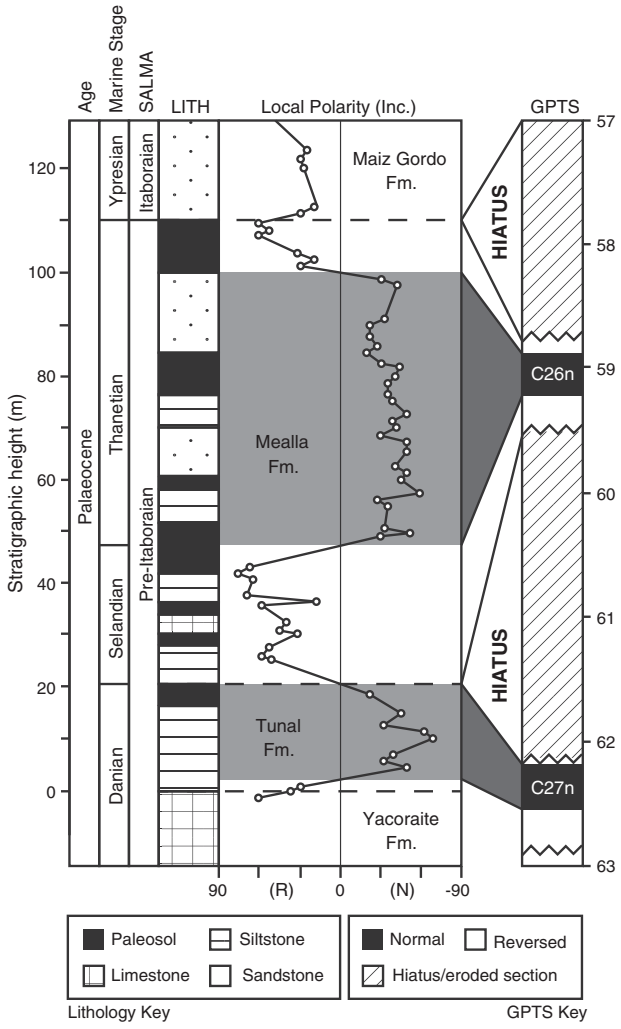

Fig. 3. Age model of Cerro Bayo section including the Tunal and Mealla Formations of the Salta Group. Correlation to the marine stages is based on palynological records (Quattrocchio et al., 1997; Quattrocchio and Volkheimer, 2000), and correlation to the South American Land Mammal Ages (SALMA) is based on limited mammalian remains (c.f. Woodburne et al., 2014). Local polarity zones are robust, and normal zones are consistent with chrons C27n (Tunal Fm.) and C26n (Mealla Fm.) of the global polarity timescale (GPTS; Gradstein et al., 2012). Dashed horizontal lines between formations indicate depositional hiatuses of varying durations (e.g., Marquillas et al., 2005).

3.2. Proxy records

The carbon isotope record ($\delta^{13}C_{org}$) through the Cerro Bayo section derived from dispersed and bifurcating paleo-root organic carbon from paleosol A-horizons identifies two carbon isotope excursions (CIEs) of roughly −2.9‰ and −4.5‰ from the local Paleocene baseline values of approximately −22‰ (Fig. 4; Data Repository Table DR2). The isotope excursions occurred in the paleosols between ~40 and 50 meters (−2.9‰; peak CIE ~59.3 Mya), or just below the Selandian–Thanetian boundary, and between ~80 and 100 meters (−4.5‰; peak CIE ~59.0 Mya), or during the early Thanetian (Fig. 4).

Climate proxy results from the geochemistry and morphology of paleosols show a rapid change in climatic conditions at Cerro Bayo concomitant with both CIEs. Mean annual temperature (MAT) estimates show a minor increase (1–2 °C) during the lower CIE, and a larger increase (3–4 °C) during the upper CIE, which is also confirmed by estimates based on paleosol clayeyness (Fig. 4; Data Repository Table DR3). These results also indicate contemporaneous changes in mean annual precipitation (MAP), with a minor decrease (100–200 mm yr^{-1}) during the lower CIE, and a larger increase (200–300 mm yr^{-1}) during the upper CIE, which is also confirmed by estimates based on paleosol depth-to-Bk horizon measurements (Fig. 4; Data Repository Table DR3).

The transient climatic shifts recorded at Cerro Bayo are also contemporaneous with shifts in vegetation composition and diversity (Figs. 4 and 5). Paleosol phytolith assemblages show a significant change in dominant vegetation type from a complex ecosystem assemblage with general forest indicators, dicots, and grasses to a substantially more limited dicot-dominated assemblage during both of the CIEs (Fig. 4). During the two CIEs, assemblages range from 16 to 27% forest indicator groups, with 73–84% dicot groups and no evidence for grasses (Fig. 6). However, outside of the CIE intervals, assemblages range from 52 to 62% forest indicator groups, with 32–47% dicot groups and 1–9% grasses (Fig. 6; Data Repository Table DR4). Phytoliths also show declines in morphotype diversity during both events with the loss of roughly half of the identifiable assemblage during the CIE intervals (Fig. 5); assemblages average ≥10 morphotypes during pre-event periods, and ≤5 morphotypes during the events themselves (Fig. 5, Data Repository Table DR4).

4. Discussion

4.1. Causes and correlations

Based on the robust age correlation of the Mealla Formation, carbon isotope data suggest a nearly −3‰ CIE roughly 50 kyr before the Selandian–Thanetian boundary, which correlates temporally to the nearly −1.5‰ CIE and substantial microfossil-community shifts in marine records that define the mid-Paleocene biotic event (Fig. 4; Bernaola et al., 2007). In addition, carbon isotope data from the Mealla Formation suggest a second, larger-magnitude CIE (−4.5‰; Fig. 4) roughly 300 kyr later during the early Thanetian for which there is no high-resolution

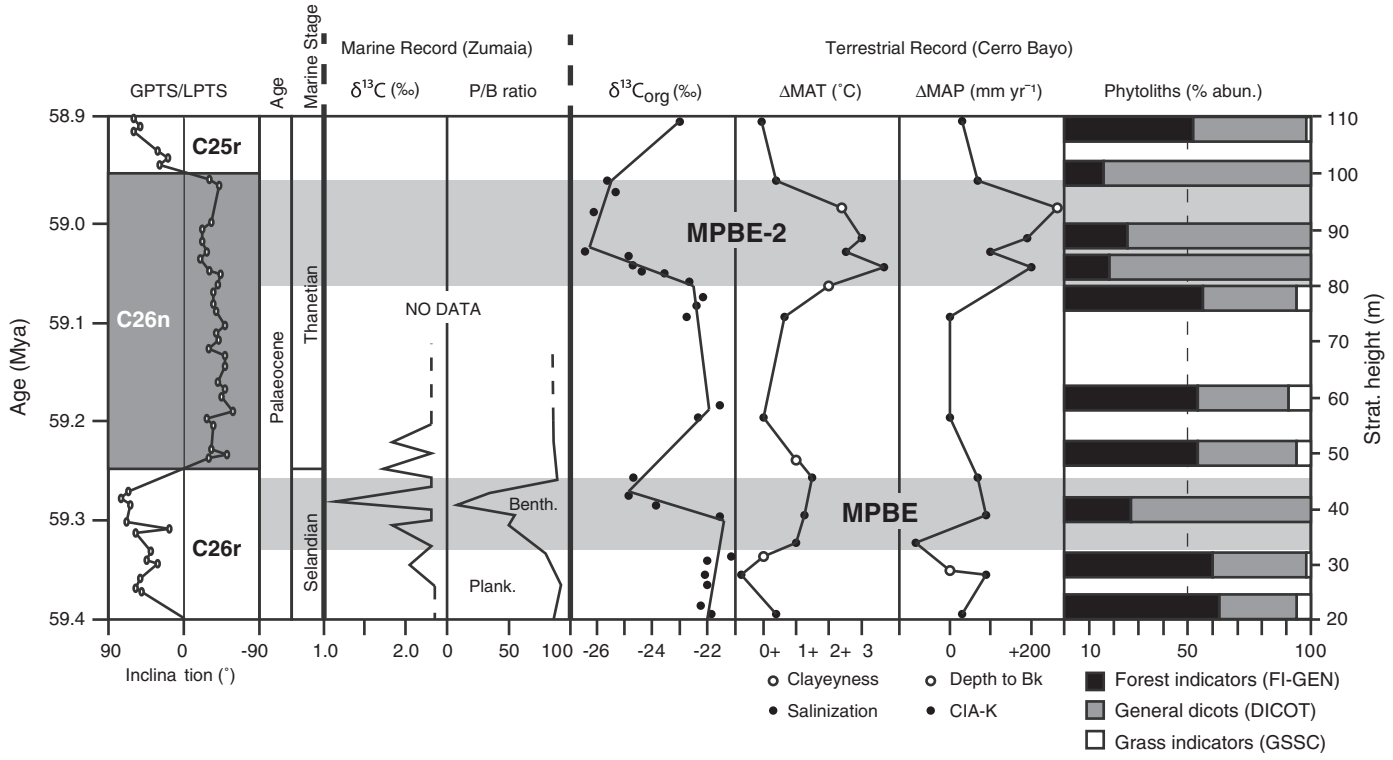

Fig. 4. Comparison of marine and terrestrial records of the mid-Paleocene biotic event (MPBE). Marine record of Zumaia locality (Spain; Bernaola et al., 2007) includes the carbon isotope composition of bulk carbonate ($\delta^{13}C$) and the ratio of planktonic to benthic foraminifera (P/B ratio), which define the MPBE interval. Terrestrial record of the Mealla Formation at the Cerro Bayo locality (this study) includes organic carbon isotope composition ($\delta^{13}C_{org}$), change in mean annual temperature from Paleocene baseline (ΔMAT), change in mean annual precipitation from Paleocene baseline (ΔMAP), and phytolith assemblage compositions. Intervals including climatic and environmental changes associated with MPBE are shaded in gray, and the two event stages are labeled (MPBE and MPBE-2).

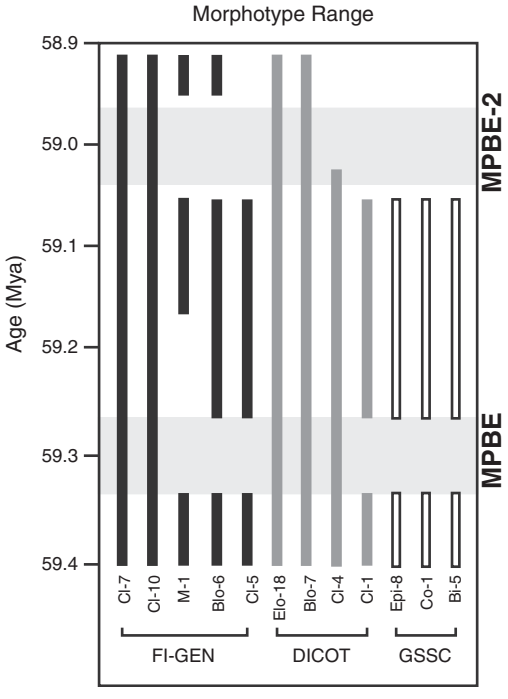

Fig. 5. Range of phytolith morphotypes through the early late Paleocene. Solid lines indicate the presence of a given morphotype, while a lack of lines indicate their absence from a time interval (see Data Repository Table DR4 for an explanation of morphotype affinities). Shaded boxes highlight MPBE and MPBE-2 time intervals defined by carbon isotope stratigraphy (Fig. 3). FI-GEN = general forest indicator morphotypes; DICOT = dicot-specific forest morphotypes; GSSC = grass silica short cells (grass morphotypes).

isotopic data in marine records (c.f., Bernaola et al., 2007; Zachos et al., 2004). This new record suggests that the carbon cycle perturbation that led to the MPBE may have occurred in two distinct stages, the second stage of which is discussed here as MPBE-2 (e.g., Fig. 4). While there are currently no isotopic data for this second CIE interval (MPBE-2) in marine records, the CIE observed in the terrestrial record does correlate temporally to an interval of other geochemical changes noted in marine records, including decreased carbonate preservation and enhanced bulk susceptibility, that are similar to those observed during the initial MPBE interval (e.g., Bralower et al., 2002; Bernaola et al., 2007). With further high-resolution carbon isotope sampling in available sediment cores during this particular interval it may be possible to identify a second CIE (denoted here as MPBE-2) in marine records as well, and thereby expand global records of the event(s) in order to improve our understanding of environmental responses to such carbon cycle changes.

The magnitude of the CIE recorded in the terrestrial sediments that correlates to the initial MPBE is roughly double that of the CIE observed in marine sediments (c.f., Bernaola et al., 2007), which is consistent with other records attributed to large-scale methane releases (e.g., Dickens, 2003; McInerney and Wing, 2011), and likely results from a combination of: 1) differences in carbon reservoir sizes (e.g., atmosphere vs. surface ocean; Kump and Arthur, 1999; Beerling, 2000), 2) isotope-effects related to changes in terrestrial climate during hyperthermals (water-stress, variable gas-exchange rates; e.g., Kraus and Riggins, 2007; Sheldon and Tabor, 2009; Diefendorf et al., 2010), and 3) preservation conditions of marine carbonates relative to terrestrial organic carbon (e.g., Bowen et al., 2004; McInerney and Wing, 2011). Floral shifts (e.g., Fig. 4) may also contribute to the amplification of the carbon isotope excursions in terrestrial organic carbon records as compared to marine records due to the potential shift in baseline carbon isotope values between different plant carbon sources (Smith et al., 2007). However, due to the lack of C_4 plant metabolisms during the Paleocene and the similar baseline range of carbon isotope values in organic

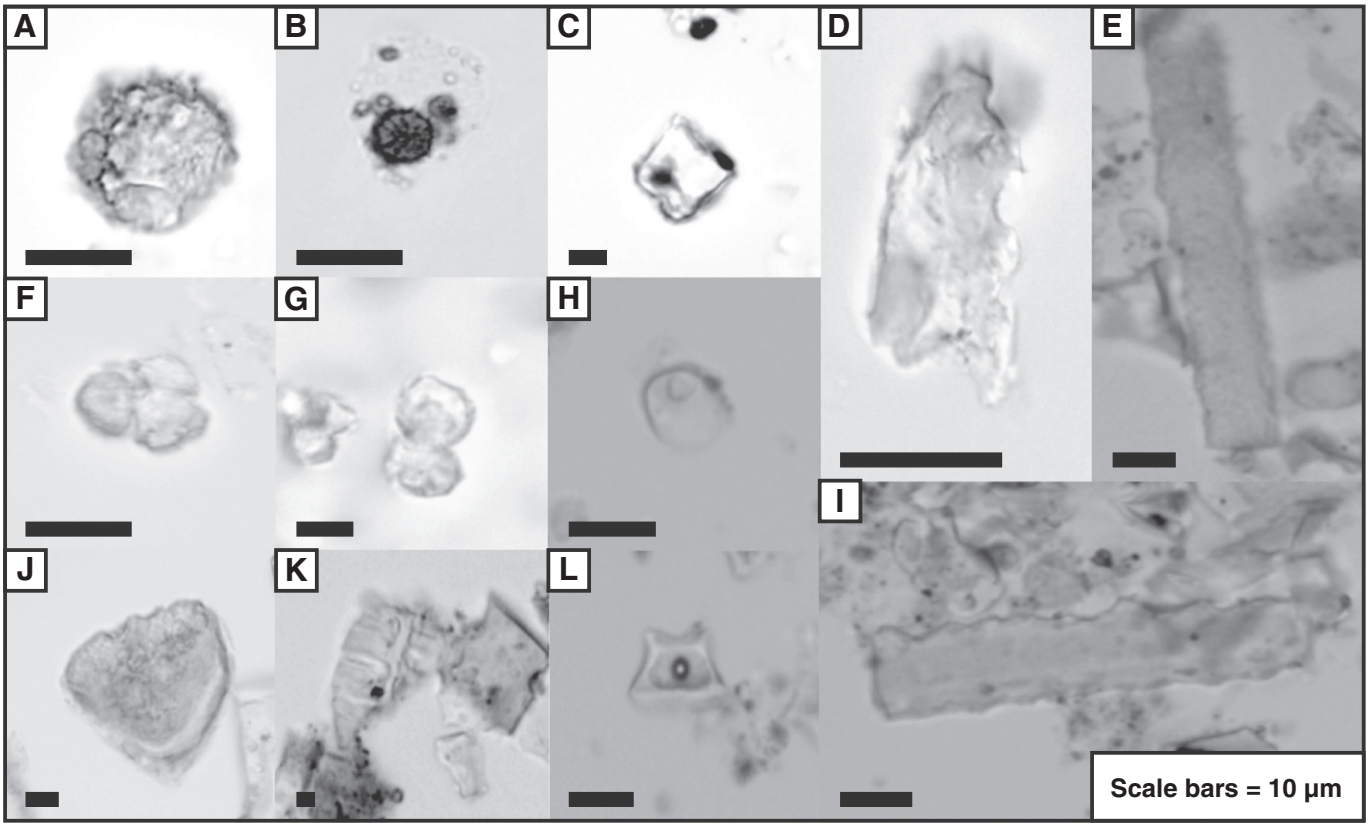

Fig. 6. Plates of phytolith morphotypes, including: A) small rugulose sphere (Cl-7; FI), B) small smooth pink sphere (Cl-4; DICOT), C) thick rectangle (Blo-7; DICOT), D) MD clump (Cl-10; FI), E) MD elongate (Elo-18; DICOT), F) compound sphere (Cl-5; FI), G) simple bilobate (Bi-5; GI), H) smooth VI sphere (Cl-1; DICOT), I) wavy elongate (Epi-8; GI), J) 3D blocky polyhedron (Blo-6; FI), K) honeycomb aggregate (M-1; FI), and L) generic rondel (Co-1; GI). All morphotypes are present in pre-event assemblages, while morphotypes depicted in panels A–E (top row) represent the MPBE/MPBE-2 assemblage (see Data Repository Table DR4). Scale bar in each image is ~10 μm.

material from most forest and closed-canopy type vegetation (e.g., Koch, 1998; Diefendorf et al., 2010), this effect is likely minimal (≤1‰; Smith et al., 2007) and therefore cannot be responsible for the entirety of the observed CIEs in these paleosols.

The magnitudes of these negative CIEs are particularly striking in the context of the global carbon cycle during the Paleocene because records of this period indicate that the atmosphere was becoming more isotopically-enriched in ^{13}C (Tipple et al., 2010), and was isotopically enriched relative to measured pre-industrial values from ice cores. Using the inferred baseline $\delta^{13}C_{atm}$ value of −4.5‰ (Tipple et al., 2010), C_3 plants that were not water-stressed should have a $\delta^{13}C_{org}$ value that was depleted by ca. −19‰ relative to that value (e.g., Sheldon and Tabor, 2009), which is very close to the measured pre- and post-MPBE excursion values from Cerro Bayo (ca. −23‰; Fig. 4). Thus, both the rapid timescale of change and magnitude of these negative CIEs relative to background Paleocene conditions suggest a substantial isotopically-depleted carbon source that could be rapidly assimilated into the carbon cycle and relatively rapidly buried, which is consistent with methane hydrate sources, the accumulation and release of which was likely high during the late Paleocene (e.g., Dickens, 2003; McInerney and Wing, 2011). Proxy data show relatively low atmospheric carbon dioxide concentrations throughout the mid-Paleocene (<500 ppmv; Beerling and Royer, 2011), but are generally very low resolution with poor coverage of transient events, which means that further high-resolution atmospheric pCO_2 records may be necessary to verify rapid carbon cycle perturbations like these suggested MPBE/MPBE-2 methane hydrate releases.

Given the relatively small initial atmospheric reservoir size, the amount of isotopically-depleted carbon necessary to produce the observed $\delta^{13}C_{org}$ shifts would be relatively modest; using the carbon accounting method described in Jahren et al. (2001), it is possible to calculate a rough estimate of how much methane would need to be released into the atmosphere to trigger the suggested $\delta^{13}C_{atm}$ shift. Making these carbon cycle perturbation estimates requires a number of assumptions, including: 1) a baseline $\delta^{13}C_{atm}$ value of −4.5‰ (Tipple et al., 2010), 2) methane with a $\delta^{13}C$ value of −60‰ (e.g., Jahren et al., 2001; Dickens, 2003), and 3) a starting atmospheric carbon reservoir of ~1500 Gt (i.e., 2.5 times the preindustrial value; e.g., Beerling and Royer, 2011), so they should not be considered fully quantitative, but nonetheless illustrate that a relatively modest injection of methane to the atmosphere could produce the observed $\delta^{13}C_{org}$ record for the MPBE intervals (Fig. 4). Assuming that each of the observed $\delta^{13}C_{org}$ shifts was due to a geologically instantaneous methane addition to the atmosphere (without oceanic buffering; e.g., McInerney and Wing, 2011), then the MPBE-1 isotopic shift of −2.9‰ would represent addition of ~83 Gt of methane-derived carbon and the MPBE-2 isotopic shift of −4.5‰ would represent an addition of ~132 Gt of methane-derived carbon to the atmosphere (c.f., Jahren et al., 2001). Given that there could be as much as 5000 Gt buried in shallow marine sediments in the modern ocean (World Ocean Report, 2010), and that seafloor methane hydrate was thought to have been much more extensive in the Paleocene (e.g., Dickens, 2003), each of these potential CIEs would represent a release of < 3% of the global budget. The similar timing of the $\delta^{13}C$ excursions in both marine and terrestrial records in different hemispheres also suggests that the release of isotopically-depleted carbon (i.e., methane hydrates) was a global rather than regional and likely multi-stage event (c.f., Bernaola et al., 2007), and that carbon cycle perturbations may have played a substantial role in the climatic and biotic changes observed during the MPBE and MPBE-2 intervals (Fig. 4).

The transient warming response observed in the terrestrial South American record for these events agrees well in terms of the expected magnitude of change with projections from marine oxygen isotope

records for the MPBE, which suggest 2–3 °C of warming (Bralower et al., 2002; Zachos et al., 2004; Lourens et al., 2005). This magnitude of warming also fits with atmospheric pCO_2-temperature sensitivity estimates based on comparable methane-release scenarios (e.g., Zeebe et al., 2009; McInerney and Wing, 2011; IPCC, 2014). Furthermore, observational and modeled results suggest regionally variable changes, such as enhanced wetting or drying trends, in local hydrologic cycling under similar greenhouse conditions (e.g., Bowen et al., 2004; Kraus and Riggins, 2007; Winguth et al., 2010). While this local climatic enhancement may partially explain the different precipitation responses for this locality during MPBE and MPBE-2 (Fig. 4), the distinct directional responses may also reflect subtle changes in the topography of nearby uplifted regions (local orographic barriers) during the late-stage Araucana Orogeny (Salfity and Marquillas, 1994; Marquillas et al., 2005). In addition to climate proxy record agreement, the stratigraphic record at Cerro Bayo shows lithologic changes toward larger and more frequent thick and coarse-grained fluvial channel deposits during the MPBE intervals (Fig. 1). These sedimentological changes suggest a shift toward less stable environmental conditions possibly caused by increased weathering and vegetation changes during the events (e.g., Fig. 4), which may be similar to the "system clearing" erosional events observed in terrestrial basins during other Paleogene hyperthermals like the Paleocene–Eocene Thermal Maximum (PETM; Foreman et al., 2012).

4.2. Biotic event on land

Changes in marine assemblages and diversity during the MPBE, such as the expansion of perturbation-tolerant benthic foraminifera at the expense of temperature-sensitive planktonic groups (Fig. 4; Bernaola et al., 2007), are also suggestive of changing ocean temperatures and carbonate chemistry, particularly in the sea surface (Bralower et al., 2002; Lourens et al., 2005). This sea-surface warming triggered a substantial top-down perturbation of marine biotic systems and the reorganization of foraminiferal and nannofossil communities (Petrizzo, 2005; Bernaola et al., 2007), which is contemporaneous with the vegetation assemblage shifts and diversity changes demonstrated by phytoliths in terrestrial records (Fig. 4).

The substantial changes in composition of local vegetation shown by this record during the MPBE/MPBE-2 events are also similar in character to the marine reorganization, as decreases in vegetation diversity and the loss of grasses and of generic forest indicator groups in favor of a specifically dicot-dominated (primarily angiosperm trees) assemblage (e.g., Figs. 4–6) are consistent with ecological responses to other major hyperthermal events such as the PETM (e.g., Wing et al., 2005). Vegetation changes during the MPBE interval were likely local environmental shifts or extirpations related to climatic conditions and not broader-scale floristic turnover events, as evidenced by the rapid return of all functional groups (Fig. 5) and the restructuring of the assemblage to its original state (Fig. 4) after the hyperthermal conditions ceased. However, vegetation changes during the MPBE-2 interval may have actually resulted in a net diversity loss similar to those observed in marine records, with the reduction in morphotypes (Fig. 5) and shifted assemblage (Fig. 4) persisting after the cessation of hyperthermal conditions. While this vegetation record is not long enough to assess the continuing character of South American floral groups fully, it does suggest that the combined MPBE/MPBE-2 intervals played an important role in the ecosystem development of the region during the late Paleocene.

Overall phytolith morphotype diversity (Fig. 5) is not directly linked to vegetation diversity, as redundancy and multiplicity are common among phytolith morphotypes (Piperno, 2006); however, significant changes in the relative abundance of functional groups, as observed through this section (Fig. 4), can signal major shifts in ecosystem composition (Strömberg et al., 2007). While the number of diagnostic morphotypes ($n = 12$) in this middle Paleocene section is low compared to other Cenozoic assemblages in South America (e.g., Strömberg et al., 2013), it is important to note that: 1) overall plant diversity during the mid-Paleocene was likely substantially lower than at other times during the Cenozoic (Wing et al., 1995; Peppe, 2010), even in the relatively higher-diversity South American floras (Jaramillo et al., 2006; Iglesias et al., 2007), and 2) the number of phytolith morphotypes increases dramatically through time with the introduction and spread of grasses, which produce more diagnostic morphotypes than other plant groups (Strömberg, 2003; Piperno, 2006). Due to both the limited abundance of grasses and the generally lower overall floral diversity of the middle Paleocene, the low number of morphotypes in this section is likely not a result of preservational biasing, and the observed trends in vegetation composition during the MPBE intervals are likely robust. These trends are also supported by evidence from other northern and central South American sites that show low overall floral diversity punctuated by periods of substantial ecosystem variability through the middle and late Paleocene (Jaramillo and Dilcher, 2000; Quattrocchio and Volkheimer, 2000; Jaramillo et al., 2006). These vegetation reconstructions also indicate the dominance of palms (a traditional climatic indicator, where cold month mean temperature >5 °C; Sakai and Larcher, 1987) in equatorial regions and the absence of palms in mid-latitude regions like the Salta Basin, which both supports moderate temperature estimates in the climatic records of Cerro Bayo and furthermore suggests that Paleocene latitudinal climatic gradients may have been more extreme (similar to modern) than previously thought (e.g., Rose et al., 2011).

5. Conclusions

Multi-proxy terrestrial paleoclimatic and paleoenvironmental records of the early late Paleocene from the southern hemisphere (Salta Basin, Argentina) suggest that the mid-Paleocene biotic event (MPBE) also impacted terrestrial systems and may have occurred in two stages. Paleosol-derived carbon isotope records show carbon cycle instability and evidence for a pair of possible large-scale methane releases during the early late Paleocene, which led to global greenhouse conditions linked to the timing of the MPBE. Terrestrial records also show resultant perturbations in the regional climate of central South America, including increased mean annual temperatures and shifts in precipitation during the identified MPBE intervals. Contemporaneous shifts in environmental conditions and substantial changes in both vegetation assemblage composition and diversity during these intervals further support the global and multistage nature of the MPBE. These shifts further provide examples of the range of possible environmental responses to potential methane releases related to future warming conditions and carbon cycle instability.

Acknowledgments

Reviews from two anonymous reviewers and Editor Finn Surlyk, and comments from Michael Woodburne have improved this manuscript greatly. We thank J. Guillou and SEGEMAR Salta (Argentina) for field assistance, and R. Van der Voo, A. Dominguez, S.Y. Smith, M. Dennis, and T. Nugent for laboratory assistance and discussion. This project was funded through the University of Michigan's Rackham Research Grants (EGH) and ExxonMobil's Geoscience Grants (JMC).

Appendix A. Supplementary data

Supplementary data to this article can be found online at http://dx.doi.org/10.1016/j.palaeo.2014.09.031.

References

Beerling, D.J., 2000. Increased terrestrial carbon storage across the Palaeocene-Eocene boundary. Palaeogeogr. Palaeoclimatol. Palaeoecol. 161, 395–405.
Beerling, D.J., Royer, D.L., 2011. Convergent Cenozoic CO_2 history. Nat. Geosci. 4, 418–420.

Bernaola, G., Baceta, J.I., Orue-Etxebarria, X., Alegret, L., Martin-Rubio, M., Arostegui, J., Dinares-Turell, J., 2007. Evidence of an abrupt environmental disruption during the mid-Paleocene biotic event (Zumaia section, western Pyrenees). Geol. Soc. Am. Bull. 119, 785–795.

Bowen, G.J., Beerling, D.J., Koch, P.L., Zachos, J.C., Quattlebaum, T., 2004. A humid climate state during the Palaeocene/Eocene thermal maximum. Nature 432, 495–499.

Bralower, T.J., Premoli Silva, I., Malone, M.J., 24 others, 2002. Proceedings of the Ocean Drilling Program, Initial Reports Leg 198 (http://www-odp.tamu.edu/publications/198_IR/198ir.htm).

Chen, S.T., Smith, S.Y., 2013. Phytolith variability in Zingiberales: a tool for the reconstruction of past tropical vegetation. Palaeogeogr. Palaeoclimatol. Palaeoecol. 370, 1–12.

Clyde, W.C., Wilf, P., Slingerland, R.L., Barnum, T., Bijl, P.K., Bralower, T.J., Brinkhuis, H., Comer, E.E., Huber, B.T., Ibanez-Mejia, M., Jicha, B.R., Krause, J.M., Schueth, J.D., Singer, B.S., Raigemborn, M.S., Schmitz, M.D., Sluijs, A., Zamaloa, M., 2014. New age constraints for the Salamanca Formation and lower Rio Chico Group in the western San Jorge Basin, Patagonia, Argentina: Implications for Cretaceous-Paleogene extinction recovery and land mammal age correlations. Geol. Soc. Am. Bull. 126, 289–306.

Cotton, J.M., Sheldon, N.D., Stromberg, C.A.E., 2012. High—resolution isotopic record of C4 photosynthesis in a Miocene grassland. Palaeogeogr. Palaeoclimatol. Palaeoecol. 338, 88–98.

Dickens, G.R., 2003. Rethinking the global carbon cycle with a large, dynamic and microbially mediated gas hydrate capacitor. Earth Planet. Sci. Lett. 213, 169–183.

Diefendorf, A.F., Mueller, K.E., Wing, S.L., Koch, P.L., Freeman, K.H., 2010. Global patterns in leaf ^{13}C discrimination and implications for studies of past and future climate. Proc. Natl. Acad. Sci. U. S. A. 107, 5738–5743.

Do Campo, M., Del Papa, C., Jiménez-Millán, J., Nieto, F., 2007. Clay mineral assemblages and analcime formation in a Palaeogene fluvial-lacustrine sequence from northwestern Argentina. Sediment. Geol. 201, 56–74.

Foreman, B.Z., Heller, P.L., Clementz, M.T., 2012. Fluvial response to abrupt global warming at the Palaeocene/Eocene boundary. Nature 491, 92–95.

Gradstein, F.M., Ogg, J.G., Schmitz, M., Ogg, G., 2012. The Geologic Time Scale 2012. Elsevier Publishing, London UK, p. 1176.

Hollis, C.J., Dickens, G.R., Field, B.D., Jones, C.M., Strong, C.P., 2005. The Paleocene-Eocene transition at Mead Stream, New Zealand: a southern Pacific record of early Cenozoic global change. Palaeogeogr. Palaeoclimatol. Palaeoecol. 215, 313–343.

Hyland, E.G., Sheldon, N.D., 2013. Coupled CO_2-climate response during the Early Eocene Climatic Optimum. Palaeogeogr. Palaeoclimatol. Palaeoecol. 369, 125–135.

Hyland, E., Smith, S.Y., Sheldon, N.D., 2013. Representational bias in phytoliths from modern soils of central North America: Implications for paleovegetation reconstructions. Palaeogeogr. Palaeoclimatol. Palaeoecol. 374, 338–348.

Iglesias, A., Wilf, P., Johnson, K.R., Zamuner, A.B., Cuneo, N.R., Matheos, S.D., Singer, B.S., 2007. A Paleocene lowland macroflora from Patagonia reveals significantly greater richness than North American analogs. Geology 35, 947–950.

Intergovernmental Panel on Climate Change, 2014. In: Stocker, T.F., Qin, D. (Eds.), Fifth Assessment Report: Climate Change. IPCC, Geneva, Switz, p. 1552.

Jahren, A.H., Arens, N.C., Sarmiento, G., Guerrero, J., Amundson, R., 2001. Terrestrial record of methane hydrate dissociation in the Early Cretaceous. Geology 29, 159–162.

Jaramillo, C.A., Dilcher, D.L., 2000. Microfloral diversity patterns of the late Paleocene-Eocene interval in Colombia, northern South America. Geology 28, 815–818.

Jaramillo, C., Rueda, M.J., Mora, G., 2006. Cenozoic plant diversity in the Neotropics. Science 311, 1893–1896.

Koch, P.L., 1998. Isotopic reconstruction of past continental environments. Ann. Rev. Earth Planet. Sci. 26, 573–613.

Kraus, M.J., Riggins, S., 2007. Transient drying during the Paleocene-Eocene Thermal Maximum (PETM): analysis of paleosols in the Bighorn Basin, Wyoming. Palaeogeogr. Palaeoclimatol. Palaeoecol. 245, 444–461.

Kump, L.R., Arthur, M.A., 1999. Interpreting carbon-isotope excursions: carbonates and organic matter. Chem. Geol. 161, 181–198.

Lourens, L.J., Sluijs, A., Kroon, D., Zachos, J.C., Thomas, E., Rohl, U., Bowles, J., Raffi, I., 2005. Astronomical pacing of late Palaeocene to early Eocene global warming events. Nature 435, 1083–1087.

Marquillas, R.A., Del Papa, C., Sabino, I.F., 2005. Sedimentary aspects and paleoenvironmental evolution of a rift basin: Salta Group (Cretaceous-Paleogene), northwestern Argentina. Int. J. Earth Sci. 94, 94–113.

McInerney, F.A., Wing, S.L., 2011. The Paleocene-Eocene Thermal Maximum: a perturbation of carbon cycle, climate, and biosphere with implications for the future. Ann. Rev. Earth Planet. Sci. 39, 489–516.

National Geophysical Data Center, 2014. Earth magnetic field values. National Oceanic and Atmospheric Administration, (http://www.ngdc.noaa.gov/geomag/magfield.shtml).

National Research Council, 2011. Understanding earth's deep past: lessons for our climate future. National Academies Press, Washington DC, USA, p. 209.

Pascual, R., 1981. El subgrupo Santa Barbara (Grupo Salta) y sus vertebrados; cronologia, paleoambientes y paleobiogeografia. Actas Congr. Geol. Argent. 8, 743–758.

Peppe, D.J., 2010. Megafloral change in the early and middle Paleocene in the Williston Basin, North Dakota, USA. Palaeogeogr. Palaeoclimatol. Palaeoecol. 298, 224–234.

Petrizzo, M.R., 2005. An early late Paleocene event on Shatsky Rise, northwest Pacific Ocean (ODP Leg 198): evidence from planktonic foraminiferal assemblages. In: Bralower, T.J. (Ed.), Proceedings of the Ocean Drilling Program, Scientific Results Leg 198 (http://www-odp.tamu.edu/publications/198_SR/102/102.htm).

Piperno, D.R., 2006. Phytoliths: a comprehensive guide for archaeologists and palaeoecologists. AltaMira, Lanham, NY USA, p. 238.

Prezzi, C.B., Alonso, R.N., 2002. New Paleomagnetic data from the northern Argentine Puna: Central Andes rotation pattern reanalyzed. J. Geophys. Res.Solid Earth 107, 1–18.

Quattrocchio, M., Volkheimer, W., 2000. Paleoclimatic changes during the Paleocene-lower Eocene in the Salta Group Basin, NW Argentina. In: Volkheimer, W., Smelka, A. (Eds.), Southern hemisphere Paleo-and Neoclimates: Key sites, data and models. Springer, New York, USA, pp. 353–367.

Quattrocchio, M., Volkheimer, W., Del Papa, C., 1997. Palynology and paleoenvironment of the "Faja Gris" Mealla Formation (Salta Group) at Garabatal Creek (NW Argentina). Palynology 21, 231–247.

Ramón, M.J., Pueyo, E.L., 2008. Cálculo de direcciones y planos virtuales paleomagnéticas: Ejemplos y comparación con otros métodos. Geotemas 10, 1203–1206.

Retallack, G.J., 2005. Pedogenic carbonate proxies for amount and seasonality of precipitation in paleosols. Geology 33, 333–336.

Retallack, G.J., 2007. Cenozoic paleoclimate on land in North America. J. Geol. 115, 271–294.

Rose, P.J., Fox, D.L., Marcot, J., Badgley, C., 2011. Flat latitudinal gradient in Paleocene mammal richness suggests decoupling of climate and biodiversity. Geology 39, 163–166.

Sakai, A., Larcher, W., 1987. Frost survival of plants: responses and adaptation to freezing stress. Springer, Berlin, GER, p. 321.

Salfity, J.A., Monaldi, C.R., 2006. Hoja Geológica 2566-IV: Metán. SEGEMAR Bol. 319, 1–80.

Salfity, J.A., Marquillas, R.A., 1994. Tectonic and sedimentary evolution of the Cretaceous–Eocene Salta Group Basin, Argentina. In: Salfity, J. (Ed.), Cretaceous tectonics of the Andes, earth evolution sciences. Friedrick Vieweg and Sohn, Berlin, GER, pp. 266–315.

Scotese, C.R., 2000. Earth System History Geographic Information System, ArcView 3.2v.2. 0C.

Sheldon, N.D., 2006. Quaternary glacial- interglacial climate cycles in Hawaii. J. Geol. 114, 367–376.

Sheldon, N.D., Tabor, N.J., 2009. Quantitative paleoenvironmental and paleoclimatic reconstruction using paleosols. Earth Sci. Rev. 95, 1–52.

Sheldon, N.D., Retallack, G.J., Tanaka, S., 2002. Geochemical climofunctions from North American soils and application to paleosols across the Eocene-Oligocene boundary in Oregon. J. Geol. 110, 687–696.

Sheldon, N.D., Costa, E., Cabrera, L., Garces, M., 2012. Continental climatic and weathering response to the Eocene-Oligocene transition. J. Geol. 120, 227–236.

Smith, F.A., Wing, S.L., Freeman, K.H., 2007. Magnitude of carbon isotope excursion at the Paleocene-Eocene thermal maximum: the role of plant community change. Earth Planet. Sci. Lett. 262, 50–65.

Staff, Soil Survey, 1999. Keys to soil taxonomy, 8th ed. Pocahontas Press, Blacksburg, Virginia (600 pp.).

Strömberg, C.A.E., 2003. The origin and spread of grass-dominated ecosystems during the Tertiary of North America and how it relates to the evolution of hypsodonty in equids. University of California Berkeley, p. 803, (PhD Thesis).

Strömberg, C.A.E., 2005. Decoupled taxonomic radiation and ecological expansion of open-habitat grasses in the Cenozoic of North America. Proc. Natl. Acad. Sci. U. S. A. 102, 11980–11984.

Strömberg, C.A.E., Werdelin, L., Friis, E.M., Sarac, G., 2007. The spread of grass-dominated habitats in Turkey and surrounding areas during the Cenozoic: Phytolith evidence. Palaeogeogr. Palaeoclimatol. Palaeoecol. 250, 18–49.

Strömberg, C.A.E., Dunn, R.E., Madden, R.H., Kohn, M.J., Carlini, A.A., 2013. Decoupling the spread of grasslands from the evolution of grazer-type herbivores in South America. Nat. Commun. 4, 1478.

Thomas, E., Zachos, J.C., 2000. Was the late Paleocene thermal maximum a unique event? GFF 122, 169–170.

Thomas, S.G., Tabor, N.J., Yang, W., Myers, T.S., Yang, Y., Wang, D., 2011. Palaeosol stratigraphy across the Permian-Triassic boundary, Bogda Mountains, NW China: implications for palaeoenvironmental transition through Earth's largest mass extinction. Palaeogeogr. Palaeoclimatol. Palaeoecol. 308, 41–64.

Tipple, B.J., Meyers, S.R., Pagani, M., 2010. Carbon isotope ratio of Cenozoic CO_2: a comparative evaluation of available geochemical proxies. Paleoceanography 25, PA3202.

Torres, M.A., Gaines, R.R., 2013. Paleoenvironmental and paleoclimatic interpretations of the late Paleocene Goler Formation, southern California, USA, based on paleosol geochemistry. J. Sediment. Res. 83, 591–605.

Turner, J.C.M., Mendez, V., Lurgo, C.S., 1979. Geologia de la region noroeste, provincias de Salta y Jujuy, Republica Argentina. Actas Congr. Geol. Argent. 7, 367–387.

Westerhold, T., Rohl, U., Donner, B., McCarren, H.K., Zachos, J.C., 2011. A complete high-resolution Paleocene benthic stable isotope record for the central Pacific (ODP Site 1209). Paleoceanography 26, PA2216.

Wing, S.L., Alroy, J., Hickey, L.J., 1995. Plant and mammal diversity in the Paleocene to early Eocene of the Bighorn Basin. Palaeogeogr. Palaeoclimatol. Palaeoecol. 115, 117–155.

Wing, S.L., Harrington, G.J., Smith, F.A., Bloch, J.I., Boyer, D.M., Freeman, K.H., 2005. Transient floral change and rapid global warming at the Paleocene-Eocene boundary. Science 310, 993–996.

Winguth, A., Shellito, C., Shields, C., Winguth, C., 2010. Climate response at the Paleocene-Eocene Thermal Maximum to greenhouse gas forcing- a model study with CCSM3. J. Clim. 23, 2562–2584.

Woodburne, M.O., Goin, F.J., Bond, M., Carlini, A.A., Gelfo, J.N., Lopez, G.M., Iglesias, A., Zimicz, A.N., 2014. Paleogene land mammal faunas of South America: a response to global climatic changes and indigenous floral diversity. J. Mamm. Evol. 21, 1–73.

World Ocean Report, 2010. Living with Oceans vol. 1. Maribus, Kiel, Germany (236 pp.).

Zachos, J.C., Kroon, D., 25 others, 2004. Early Cenozoic extreme climates: the Walvis Ridge transect. Proceedings of the Ocean Drilling Program, Leg 208 (http://www-odp.tamu.edu/publications/208-IR/208ir.htm).

Zachos, J.C., McCarren, H., Murphy, B., Rohl, U., Westerhold, T., 2010. Tempo and scale of late Paleocene and early Eocene carbon isotope cycles: implications for the origin of hyperthermals. Earth Planet. Sci. Lett. 299, 242–249.

Zeebe, R.E., Zachos, J.C., Dickens, G.R., 2009. Carbon dioxide forcing alone insufficient to explain Palaeocene-Eocene Thermal Maximum warming. Nat. Geosci. 2, 576–580.